scientific reports

Check for updates

OPEN

# Effects of applied magnetic fields on the performance of magnetoplasmadynamic thrusters

Haewon Shin[1], Jeongho Kim[2], Jaeyeon Hwang[2], Kil-Byoung Chai[1]✉ & Holak Kim[2]✉

**Since the performance of MPD thrusters is highly dependent on the applied magnetic field, we experimentally investigated the effects of magnetic field geometry. Thrust, specific impulse, and ion energy distribution were measured under various operating conditions. The results indicate that the magnetic field configuration of ring–type permanent magnets with a magnetic null point may limit effective ion acceleration, leading to reduced thrust while the permanent magnet produces a stronger applied magnetic field ($B_A$: 0.175 T) than the electromagnet ($B_A$: 0.016–0.065 T). This reduction could be attributed to disrupted axial electron mobility and shortened magnetic field line lengths near the magnetic null point. For the electromagnet configuration, thrust increased more significantly with discharge current at a lower argon flow rate (500 sccm) and a higher electromagnetic coil current (40 A). When the discharge current was increased to 300 A under the aforementioned conditions with an input power of 15 kW, the maximum thrust of 436 mN and the specific impulse of 2935 s were obtained. In the permanent magnet configuration, at a flow rate of 600 sccm and an input power of 10 kW, the thrust and specific impulse were 234 mN and 1340 s, respectively. In the comparable operating ranges, these values were approximately 28% and 15% lower, respectively, than those obtained with the electromagnet configuration. Besides these observations, the current-voltage (I–V) characteristics also show a dependence on the magnetic field configuration. The permanent magnet configuration exhibited a higher discharge voltage at a given discharge current, leading to reduced current levels under the same input power relative to the electromagnet configuration. The findings highlight the dominant influence of the magnetic field geometry on the thruster performance, along with the contributions of the discharge current and the argon flow rate.**

**Keywords** AF–MPD thruster, Magnetic field, Thruster performance, Permanent magnet, Electromagnet

Space electric propulsion is crucial to advanced space exploration, offering a high specific impulse[1,2]. Among these technologies, magnetoplasmadynamic (MPD) thrusters are particularly promising due to their scalability from kW to MW power levels, high thrust density, and high specific impulse[1–7]. As the demand for reliable, high-power propulsion in deep-space missions continues to grow, further advancements in MPD thruster technology become increasingly critical[4,8]. However, progress in MPD thruster development has been relatively slow in recent decades, primarily due to the high power requirements for efficient operation[6,9]. Thus, resolving the challenges of supplying sufficient power to thruster systems is essential for the successful implementation of MPD thrusters[6,10]. Recent advancements in space nuclear fission power and nuclear-electric propulsion (NEP) systems have drawn increasing attention to high-power electric propulsion technologies, including MPD thrusters[11–13]. In the United States and other countries, compact and efficient fission reactors are being developed for potential use in space applications[14,15]. Meanwhile, various international research efforts are exploring the feasibility of nuclear-electric propulsion for long-duration interplanetary missions[16]. Ongoing developments in these technologies are expected to facilitate the effective implementation of MPD thrusters in deep-space missions, where the magnetic field configuration plays a significant role in thruster performance[4,12].

Applied-field magnetoplasmadynamic (AF-MPD) thrusters utilize external magnetic fields to accelerate ionized propellants[1,7] with two primary methods for generating magnetic fields: permanent magnets and electromagnets[17–19]. Since the early stages of MPD thruster development in the 1960s, electromagnets have

[1]Nuclear Physics Application Research Division, Korea Atomic Energy Research Institute, 111 Daedeok-daero 989beon-gil, Yuseong-gu, Daejeon 34057, Republic of Korea. [2]Department of Aerospace Engineering, Pusan National University, Busandaehak-ro 63 beon-gil 2, Geumjeong-gu, Busan 46241, Republic of Korea. ✉email: kbchai@kaeri.re.kr; holakkim@pusan.ac.kr

served as the primary means of generating applied magnetic fields in AF-MPD thrusters[20]. During the 1980s and 1990s, performance optimization efforts utilizing electromagnets were conducted through high-power MPD experiments. More recently, research on electromagnet-based AF-MPD thrusters has continued, including investigations into the Lorentz Force Accelerator (LiLFA) at Princeton University and the SX3 thruster at the University of Stuttgart[21,22]. Active research on the application of permanent magnets began relatively later, around the 1990s, with experimental studies conducted by researchers at the University of Tokyo[18]. Due to limitations in magnetic field strength and controllability, permanent magnets have primarily been investigated for low- to mid-power MPD systems.

Each method presents distinct advantages and limitations. Permanent magnets[18,23,24] and electromagnets[22,25–29], which are commonly used to generate magnetic fields in applied field MPD thrusters, differ significantly in structural simplicity, controllability, and magnetic field topology. A detailed comparison between the two configurations is presented in Table 1. As the geometry of the magnetic field influences the behavior of charged particles, it is expected to have a direct impact on both plasma characteristics and thruster performance.

Despite its critical influence on thruster performance, detailed studies on the effects of permanent magnets and electromagnets in MPD thrusters remain limited. Most prior research has primarily focused on thruster performance in relation to magnetic field strength, without providing a comprehensive analysis of the impacts of magnetic field geometry on thrust. Recent studies[30,31] have highlighted the importance of magnetic field topology in determining MPD thruster performance, particularly its role in governing plasma confinement and electromagnetic acceleration processes. Extending previous studies into plasma confinement and electromagnetic acceleration processes, the present study experimentally demonstrates the significant influence of magnetic field geometry on MPD thruster performance, particularly with respect to differences between electromagnet and permanent magnet configurations.

The objective of this paper is to conduct a comparative study on the performance of magnetic field configurations by permanent magnets and electromagnets in low-power MPD thrusters. Although the experiments were conducted using a low-power MPD thruster, the findings are expected to be applicable to high-power MPD thrusters due to their scalability. By evaluating thruster performance under various experimental conditions, the results are anticipated to offer valuable insights into the design of MPD thrusters for future space missions.

## Results

The experiments were carried out to evaluate the performance and discharge characteristics of the AF-MPD thruster using electromagnets and permanent magnets as external magnetic field sources. For the electromagnet configurations, experiments were conducted at argon flow rates of 500, 750, and 1000 sccm, with thruster performance evaluated at discharge currents ranging from 100 to 300 A in 50 A increments. In the permanent magnet configuration, experiments were conducted at discharge currents ranging from 138 A to 290 A and argon flow rates of 600, 800, and 1000 sccm, covering a similar operational range to that of the electromagnet case.

*Discharge characteristics.* The I–V curve characteristics as a function of discharge current were compared between the electromagnet and permanent magnet cases, as shown in Fig. 1. Figures 1a–c represent I–V curves obtained for the electromagnet cases, while Fig. 1d presents the I–V curves measured for the permanent magnet case. At discharge currents below a transition current, which was observed near 100 A in the present experiments, increased thermionic emission from the hot cathode leads to a reduction in discharge voltage. When the discharge current exceeds the transition current, the voltage increases, indicating a transition from a non-thermal to a thermal arc. This transition aligns with the DC arc discharge theory, where a thermal arc regime characterized by local thermodynamic equilibrium is established above a transition current, and field emission dominates over thermionic emission[32]. In the non-thermal region, the I–V curve exhibits a negative slope as the current increases while the slope becomes positive as the discharge enters the thermal arc regime. In the present experiments, both the electromagnet and permanent magnet configurations exhibited this transition near 100 A, indicating that the I–V characteristics follow the typical arc behavior regardless of the magnetic field geometry.

In Figs. 1a–c, the I–V curves are compared based on Ar flow rates and electromagnetic coil currents. At flow rates of 750 sccm and 1000 sccm, the I–V curves exhibited similar characteristics under identical operating conditions. At the lowest flow rate of 500 sccm, a significant increase in voltage was observed as

| Feature | Permanent magnet | Electromagnet |
|---|---|---|
| Power requirement | No external power<br>Simple system<br>Ideal for long-term missions | Electrical power required<br>Increased system complexity |
| Controllability | Fixed magnetic field<br>Low operational flexibility | Adjustable magnetic field<br>Thrust and $I_{sp}$ controllability |
| Magnetic field topology | Substantial radial field<br>Magnetic null point<br>(ring-shaped configuration) | Dominant axial field<br>No magnetic null within discharge channel |

**Table 1**. Summary of the main features of permanent-magnet and electromagnet systems applied to MPD thrusters.

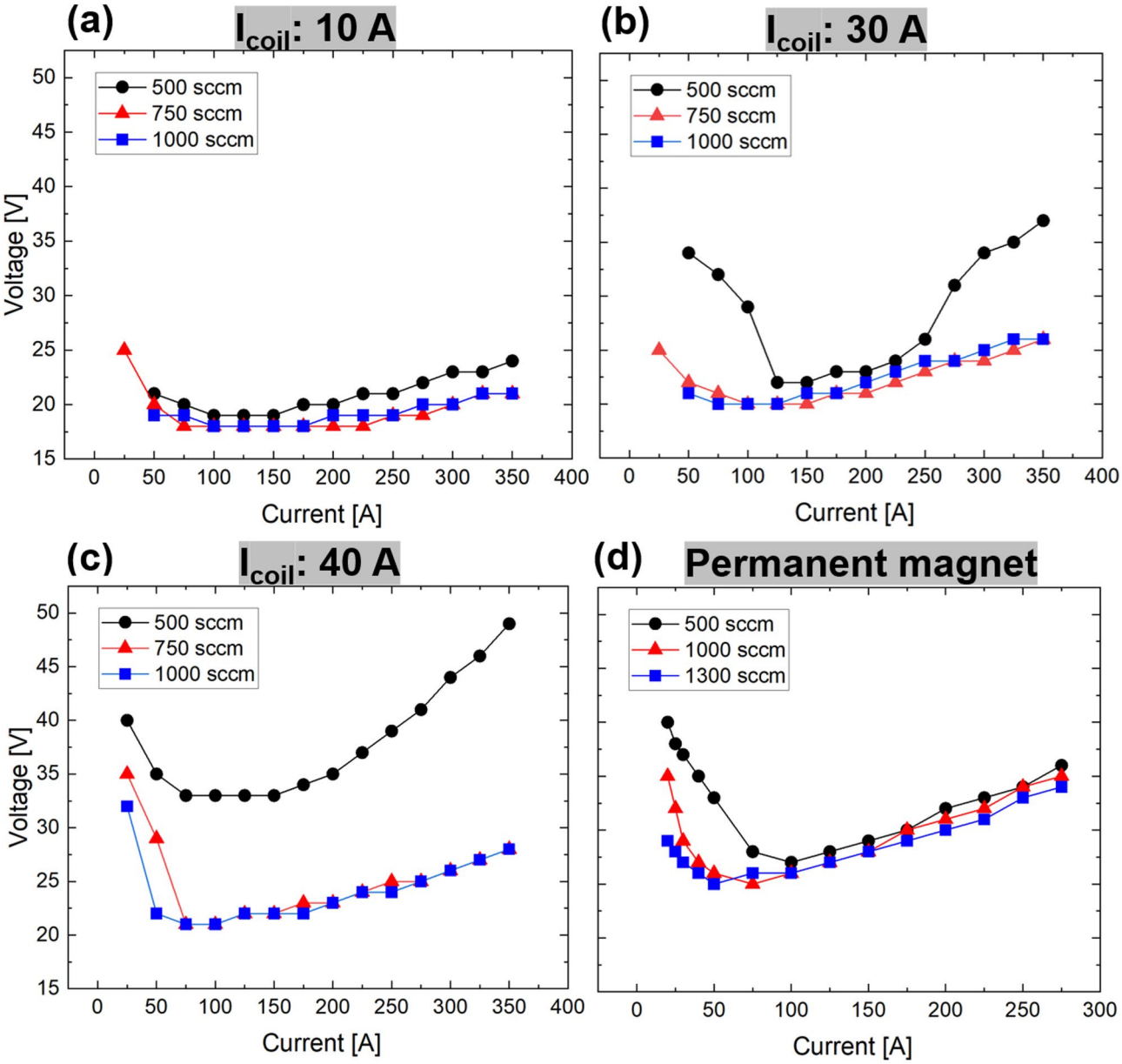


**Fig. 1**. Comparison of the thruster I–V characteristics at different argon flow rates under various magnetic field configurations: (**a**) electromagnet configuration with coil current $I_{coil}$: 10 A, (**b**) $I_{coil}$: 30 A, (**c**) $I_{coil}$: 40 A, and (**d**) the permanent magnet configurations. At 750 sccm and 1000 sccm flow rates, the I–V curves are similar. At 500 sccm, voltage increases significantly with coil current. The permanent magnet configuration shows minimal flow rate dependence at discharge currents above 100 A.

the electromagnetic coil current increased. Notably, when the electromagnet coil current was 40 A, the voltage exhibited a steeper rise as the discharge current increased compared to the other cases. For the permanent magnet configuration, at discharge currents exceeding 100 A, the voltage increased with rising current, while the effect of flow rate remained negligible, as shown in Fig. 1d. The permanent magnet configuration showed higher voltages at the same discharge current compared to the electromagnet configuration at 750 sccm and 1000 sccm. The higher voltage in the permanent magnet configuration at a given discharge current (Fig. 1d) leads to a reduction in discharge current under equal input power, which could result in lower thrust compared to the electromagnet configuration.

*Thruster measurement results.* In this subsection, the performance of the AF-MPD thruster was evaluated for different magnetic field configurations generated by the electromagnet and the permanent magnet. Thrust versus $IB_A$ (the product of discharge current and applied magnetic field) was selected for comparison, as previous studies have indicated that thrust in AF-MPDTs is proportional to this parameter[19,33]. Given that variations in Ar flow rate and the magnetic field structures affect the I–V curve characteristics, thrust curves as a function of input power are also presented.

Figures 2a and b present thrust as a function of $IB_A$ for configurations utilizing the electromagnet and the permanent magnet, respectively. While the operational discharge current range is comparable for both electromagnet and permanent magnet cases, the $B_A$ in the permanent magnet case is approximately 3–10 times higher than that of the electromagnet, resulting in differences in the $IB_A$ range, expressed in N/m. For the permanent magnet configuration, thrust exhibited a linear increase with $IB_A$, and higher argon flow rates resulted in greater thrust, as shown in Fig. 2b. At a low electromagnet coil current ($I_{coil}$: 10 A), thrust also exhibited a linear increase with $IB_A$, following a trend similar to that of the permanent magnet. Additionally, the higher flow rate (1000 sccm) led to a steeper increase in thrust compared to the lower flow rate (500 sccm). Interestingly, at a high coil current ($I_{coil}$: 40 A), thrust increased more sharply with $IB_A$ at a lower flow rate than at a higher flow rate. Moreover, when $IB_A$ exceeded 12 [N/m], thrust at the lower flow rate surpassed that at the higher flow rate case.

Thrust and specific impulse $I_{sp}$ were evaluated as a function of input power, as shown in Fig. 3. In both cases of the electromagnet and the permanent magnet, higher argon flow rates resulted in greater thrust at the same input power. For specific impulse, the permanent magnet configuration exhibited a linear increase with power, with no apparent dependence on flow rate. Similarly, in the electromagnet configuration at flow rates of 750 sccm and 1000 sccm, the effect of argon mass flow on $I_{sp}$ was negligible. However, at a lower flow rate of 500 sccm, $I_{sp}$ increased significantly at the same input power and showed a steep increase with increasing power. The maximum thrust of 436 mN and the maximum $I_{sp}$ of 2935 s were achieved at an argon flow rate of 500 sccm, $I_{coil}$ of 40 A, and an input power of 15 kW.

*Ion energy distributions measured by RPA*. The ion energy distributions were measured using a retarding potential analyzer (RPA) for the electromagnet configurations. The normalized ion energy distribution function (IEDF) for each flow rate is presented in Fig. 4. The peak ion energy exhibited an increasing trend with higher discharge current and electromagnet coil current. At a coil current of 10 A, the peak ion energy ranged between 21 eV and 35 eV across all flow rate cases. For a coil current of 40 A, the peak ion energy varied from 25 eV to 41 eV for the argon flow rates of 750 sccm and 1000 sccm. Notably, the peak ion energy increased as the argon flow rate decreased. In particular, at a flow rate of 500 sccm, the ion energy demonstrated a substantial increase compared to other flow rate conditions, with a maximum peak ion energy of 63 eV obtained at a discharge current of 300 A and a coil current of 40 A. The increase in peak ion energy observed at lower mass flow rates could be associated with the increase in the voltage. A similar trend was also observed in the permanent-magnet configuration, although the increase in peak ion energy at lower mass flow rates was less pronounced. At reduced flow rates, the lower electron density near the anode enhances the anode sheath voltage fall, which in turn increases the discharge voltage[22]. This higher potential difference may lead to stronger ion acceleration and thus higher peak ion energy. In addition, lower argon flow rates could reduce collisionality, allowing ions to retain more energy under the same magnetic field and discharge current, which may lead to the higher peak ion energy.

*Thruster efficiency*. Thruster efficiency under various experimental conditions is plotted against specific impulse $I_{sp}$ in Fig. 5. Under comparable argon flow rate conditions, the efficiency and thrust density in the permanent magnet cases were lower than observed in the electromagnet cases. The efficiency and $I_{sp}$ for the

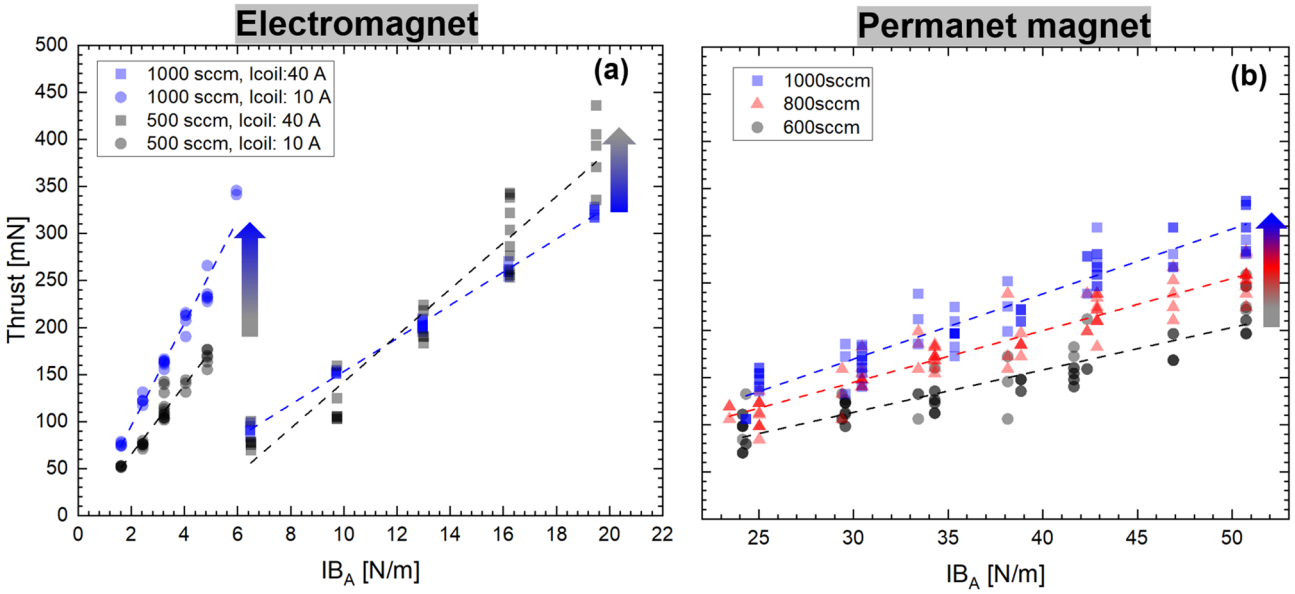


**Fig. 2**. Thrust as a function of the product of magnetic field strength and discharge current ($IB_A$) for (**a**) the electromagnet and (**b**) the permanent magnet configurations. For the electromagnet case (**a**), 10 A and 40 A data are shown by circle (●) and square (▪) symbols, respectively. The permanent magnet provides a stronger magnetic field, resulting in higher $IB_A$ (N/m) values. However, these higher $IB_A$ values do not yield higher thrust because its magnetic null point restricts efficient plasma acceleration. A more detailed explanation is provided in the discussion section.

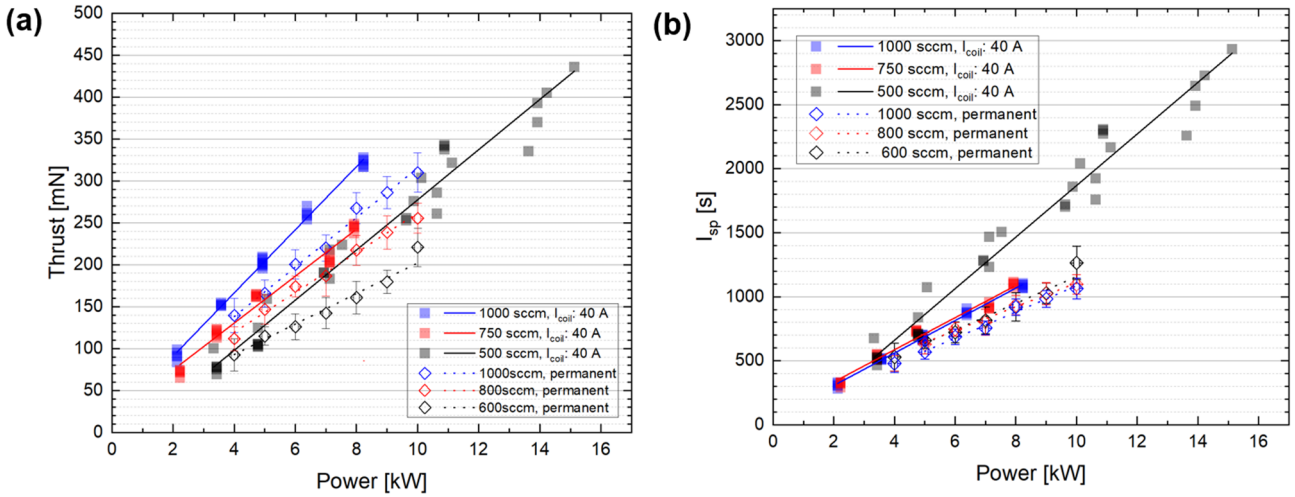


**Fig. 3**. (**a**) Thrust and (**b**) specific impulse ($I_{sp}$) as a function of input power for both electromagnet and permanent magnet configurations. Thrust increased with input power, and higher argon flow rates resulted in higher thrust. $I_{sp}$ showed a linear increase with power in the permanent magnet case, independent of flow rate. In the electromagnet case, $I_{sp}$ increased significantly with power only at the low flow rate of 500 sccm.

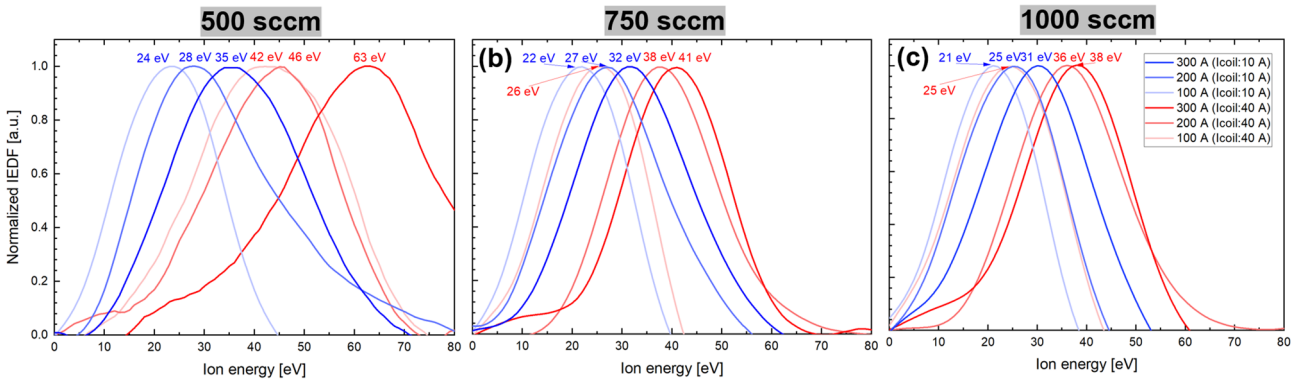


**Fig. 4**. Normalized ion energy distribution functions (IEDFs) measured using a retarding potential analyzer (RPA) for the electromagnet configuration at various argon flow rates. Peak ion energy increased with both discharge current and coil current, and was highest at the lowest flow rate (500 sccm). At a coil current of 10 A, the peak ion energy ranged between 21 eV and 35 eV. At the coil current of 40 A, the peak ion energy reaches 63 eV at the flow rate of 500 sccm, which is 66% higher than that observed at the flow rate of 1000 sccm (38 eV). This result indicates that a higher potential difference at lower flow rates leads to stronger ion acceleration.

permanent magnet case ranged between 3.4% and 19% and 401–1156 s, respectively, corresponding to an input power of 4–10 kW. The thrust-to-power ratio was primarily concentrated between 20 and 40 mN/kW. Meanwhile, in the magnetic field geometry of the electromagnet, the thrust-to-power ratio was slightly higher, typically ranging from 25 to 45 mN/kW. The highest thrust-to-power ratio of 46.5 mN/kW was achieved at a high argon flow rate (1000 sccm) and low input power (2.1 kW), whereas the maximum efficiency of 42% was obtained at a low flow rate (500 sccm) and high input power (15 kW).

## Discussion

The results demonstrate that the performance characteristics of the thruster are significantly affected by the geometry of the external magnetic field, which varies depending on the type of magnet employed. Given that acceleration mechanisms in MPD thrusters are inherently interdependent on complex electromagnetic and gas-dynamic processes, a comprehensive understanding of how magnetic field configurations affect plasma behavior is essential for optimizing thruster performance[30,31].

Among the key factors determining thruster performance, I–V characteristics play a critical role, as they affect thruster efficiency by governing the power consumption required for operation. In particular, the magnetic field geometry, along with discharge current and argon flow rate, significantly impacts plasma properties and

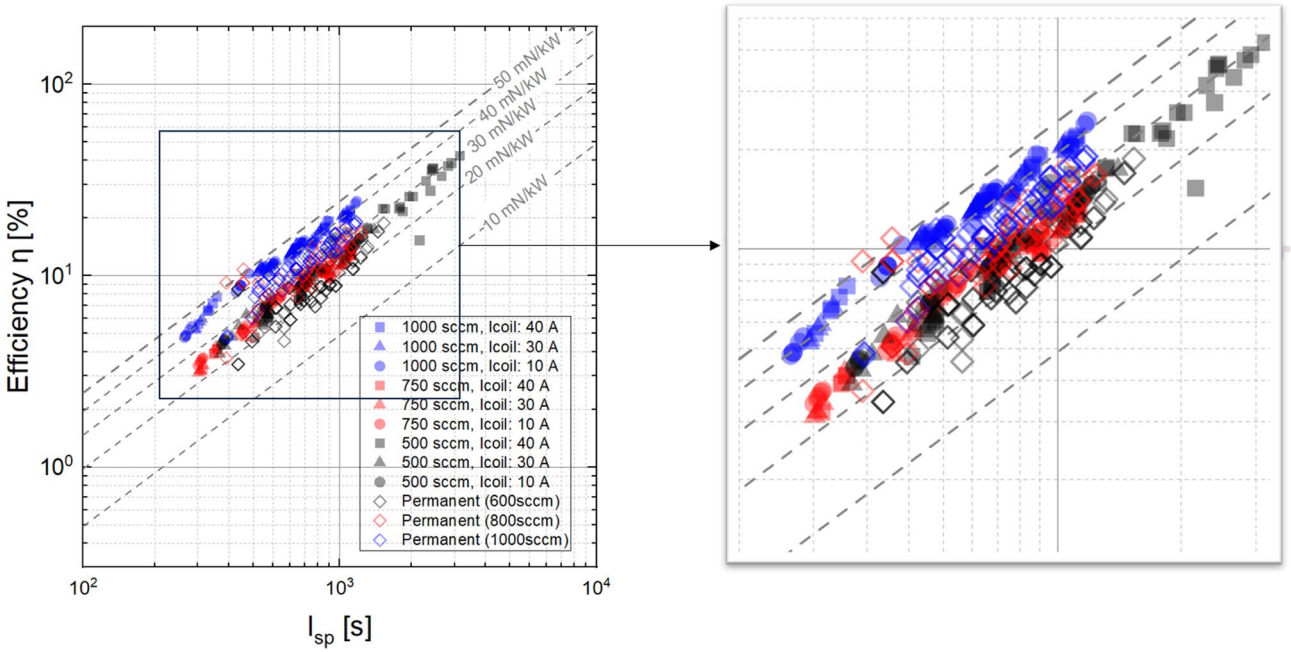


**Fig. 5**. Thruster efficiency of the low-power AF-MPD thruster plotted as a function of $I_{sp}$ under various magnetic field configurations. The electromagnet configuration generally exhibited higher efficiency and thrust-to-power ratios than the permanent-magnet configuration under comparable argon flow rates (500–1000 sccm) and input powers (2–15 kW). For the permanent-magnet case, the efficiency ranged from 3.4 to 19%, and $I_{sp}$ from 401 to 1156 s, whereas the electromagnet configuration achieved up to 42% efficiency and a maximum thrust-to-power ratio of 46.5 mN/kW.

the resulting I–V curve. Consequently, a comprehensive understanding of the I–V characteristics under various conditions is essential for optimizing thruster performance.

The experimental results obtained under different magnetic field configurations indicate that, for the same input power, the electromagnet configuration generates higher thrust than the permanent magnet configuration. This difference can be attributed to the I–V characteristics, where the permanent magnet configuration results in a higher voltage being applied to the cathode at a given discharge current, as shown in Fig. 1. Since thrust is primarily influenced by discharge current, the lower current levels observed in the permanent magnet case at the same input power lead to lower thrust compared to the electromagnet case under similar mass flow rates (see Fig. 3a). Additionally, these results can be interpreted in terms of particle behavior under different magnetic field configurations. In the permanent magnet configuration, despite its higher $B_A$, the presence of a magnetic null point generates a strong radial magnetic field near the thruster axis (Fig. 6c), which shortens the field-line length in the discharge channel, disrupts axial electron mobility, and consequently weakens the induced electric field, thereby impeding ion acceleration. Furthermore, a shorter field line length in the thruster channel may reduce the ionization rate, leading to lower plasma density. Consequently, the reduced ionization may lead to a lower local density, which degrades overall thruster performance[34,35].

As demonstrated in the results, across all magnetic field configurations, the total voltage exhibited an increasing trend with both the strength of the magnetic field and the discharge current in the primary operational regime above 100 A. In the thrust versus $IB_A$ graph for the electromagnet configuration, as depicted in Fig. 2, thrust consistently increased with discharge current under all conditions for both the electromagnet and permanent magnet configurations. In addition, in most cases, for a given $B_A$ and discharge current, a higher flow rate resulted in greater thrust. A noteworthy observation is that under higher $B_A$ conditions ($I_{coil}$: 40 A), thrust exhibited a more pronounced increase with discharge current in the low mass flow rate case compared to the high mass flow rate case. Consequently, for discharge currents above 200 A, the thrust at a lower mass flow rate exceeded that at a higher mass flow rate for the same discharge current. The observed trend can be understood through the semi-empirical voltage model, which is mainly affected by the magnetic field[22,36,37]. The semi-empirical voltage model shows the relationship between discharge voltage and current in the AF-MPD thrusters. The model explains the total discharge voltage as a combination of resistive losses, electrode-sheath contributions, and back electromotive voltage associated with the motion of plasma. Since thruster performance is primarily influenced by the I–V characteristics, the back electromotive voltage, which is responsible for plasma acceleration, plays a key role in thruster performance. The back electromotive voltage scales linearly with the discharge current and quadratically with the applied magnetic field, while showing an inverse dependence on the mass flow rate as in Ref[22]. Accordingly, under a fixed applied magnetic field, the contribution of the discharge current to the back electromotive voltage becomes more pronounced at lower mass flow rates, resulting in a steeper increase in thrust with discharge current as shown in Fig. 2.

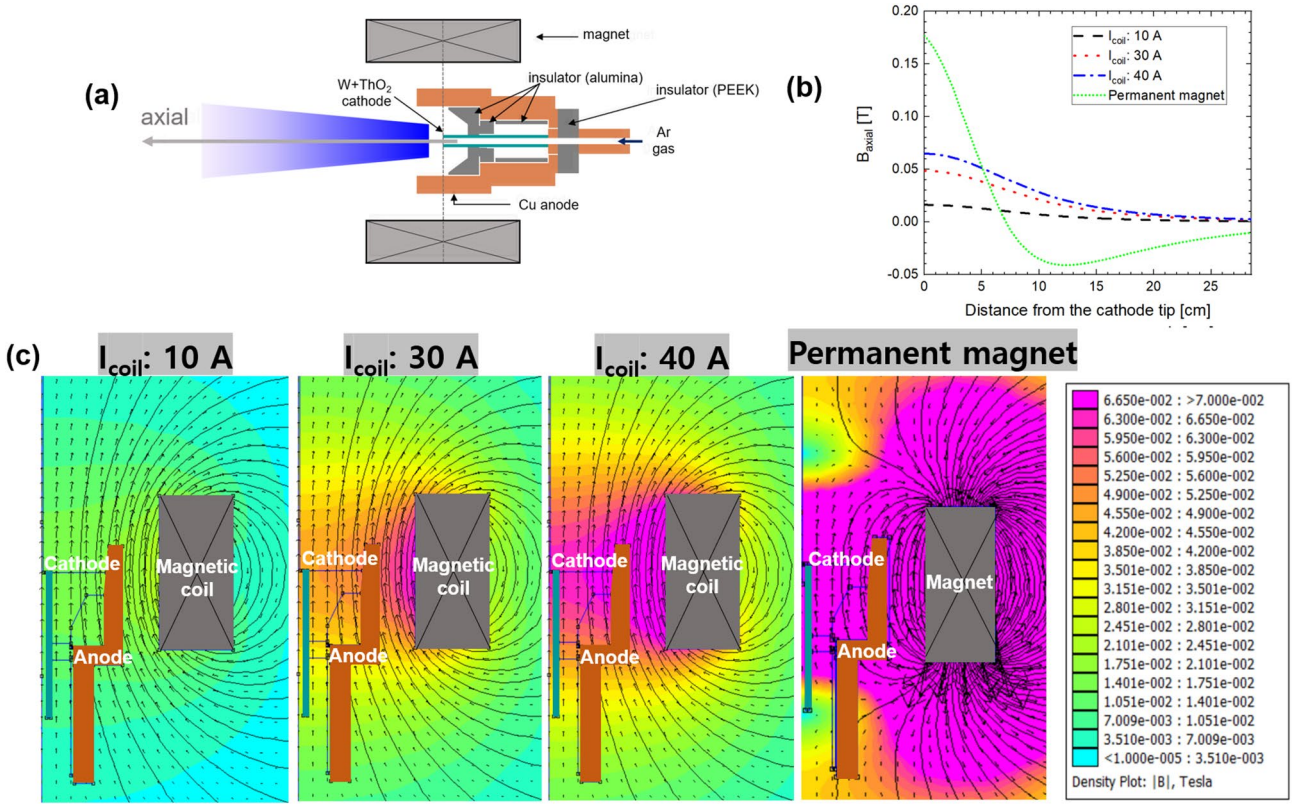


**Fig. 6**. (**a**) Structure of the AF-MPD thruster, (**b**) axial magnetic flux density along the channel, and (**c**) magnetic field distributions for the electromagnet and permanent magnet configurations. The thruster consists of a water-cooled copper anode, thoriated tungsten cathode, and three alumina insulators. External magnetic fields are applied using either the electromagnet or the permanent magnet. FEMM simulations show an axially dominant field for the electromagnet configuration and a strong radial component near the null point in the permanent magnet configuration.

Isolating the specific influence of magnetic-field geometry remains an important topic for understanding the physics of AF-MPD thrusters. To decouple the effects of magnetic field strength and geometry, comparisons at comparable magnetic field strengths are required. In the present study, the electromagnet provided a lower magnetic field strength than the permanent magnet, which limited the ability to perform a fully decoupled analysis. In follow-up research, the electromagnet will be upgraded so that it can provide a magnetic field strength comparable to that of the permanent magnet, allowing investigation of the independent influence of magnetic field geometry.

## Summary and conclusion

A comparative analysis of AF-MPD thruster performance using permanent magnets and electromagnets was conducted. Experimental investigations were carried out by varying discharge currents, flow rates, and magnetic field configurations to evaluate thruster performance, including ion energy distributions and thruster efficiency. The results indicated that while the permanent magnet configuration generated a higher $B_A$, the presence of a magnetic null point restricted effective ion acceleration. It should be noted that the axially magnetized ring-type magnet employed in this study generates a magnetic null point on the central axis of the discharge channel, which is a feature specific to this configuration. In the electromagnet configuration, improved thrust and efficiency was observed, particularly at lower mass flow rates and higher applied magnetic fields. Additionally, the I–V characteristics, which varied with flow rate and magnetic field strength, played a crucial role in performance. The underlying physical interpretation is as follows[22]: as the discharge current and magnetic field strength increase, plasma pinching along the thruster centerline is enhanced, thereby reducing the flux of electrons entering the near-anode region. This effect becomes more pronounced at lower flow rates and stronger magnetic field strength, leading to enhanced thruster performance, as demonstrated by the semiempirical voltage model and the measured ion energy distributions. For a comparable power range, scalability within a fixed electromagnet configuration has been reported in Ref[22]. The study also showed a good agreement between experimental data and the trends predicted by the semi-empirical thrust and voltage model. Our experimental results exhibit similar trends, supporting the expectation that this scalability can extend to high power regimes, as evidenced by the linear relationship between thrust and $IB_A$ observed in the present study (see Fig. 2), which is consistent with MW-class MPD thruster scaling studies reported in Refs[33,38].

These findings highlight the critical role of magnetic field geometry in the design of MPD thrusters. While a stronger magnetic field generally enhances performance, the specific field topology has a significant influence on plasma behavior and ion acceleration efficiency. Thus, optimizing MPD thruster performance necessitates a careful selection of magnet type, discharge conditions, and system parameters to achieve an optimal balance among thrust, efficiency, and power consumption.

## Methods

*MPD thruster and experimental setup.* This section presents an overview of the low-power AF-MPD thruster used in this study, detailing its structural design, the magnetic field geometry generated by the permanent magnet or electromagnet, the thrust measurement setup, and the vacuum facility.

*Thruster discharge channel and magnetic field geometry.* The AF-MPD thruster used in this work consists of a thoriated tungsten (2%) cathode, a copper anode, and three alumina insulators[39,40]. The cylindrical cathode, with an outer diameter of 12 mm, is enclosed by an anode with an inner diameter of 80 mm. The total length of the cathode is 110 mm, and its exposed length can be adjusted. Argon is used as the propellant gas and is supplied through the cathode. Both the anode and cathode are equipped with a water-cooling circuit to regulate temperature and dissipate the substantial heat generated by the DC power input. The schematic layout of the thruster is depicted in Fig. 6a.

The electromagnet and the permanent magnet were utilized as sources of external magnetic fields to examine the effects of magnetic field geometry on thruster performance. Both magnets were designed in a ring shape with identical dimensions and were equipped with a water-cooling jacket on the plasma-facing side to protect them from the heat flux generated by the plasma. During continuous thruster operation for more than 1 h, no degradation in thrust performance was observed despite continuous exposure to the heat flux generated by the plasma, indicating that the water-cooling jacket effectively maintained the magnetic field stability. The axial positions of the magnet centers were aligned near the tip of the cathode. In the electromagnet configuration, the center of the magnet was aligned with the tip of the cathode, whereas in the permanent magnet configuration, it was positioned at the end of the insulator, 13 mm from the cathode tip. The electromagnet was constructed by winding 300 turns of AWG 7 wire, which has a cross-sectional area of 10 $mm^2$. To ensure stable operation, the current supplied to the electromagnetic coil was limited to 40 A in accordance with the ampacity of the wire. The thruster performance with the electromagnet was evaluated under three operating conditions, with coil currents of 10 A, 30 A, and 40 A. The permanent magnet used in this study is an axially magnetized ring-type magnet whose two flat surfaces correspond to the N and S poles. Owing to this geometry, the axial magnetic field exhibits a null point on the central axis of the discharge channel. This characteristic is specific to the present magnet configuration, and permanent magnets with different geometries or placements may not exhibit such a null point. The permanent magnet was made of neodymium–iron–boron (Nd–Fe–B, grade N38H) with a magnetic remanence ($Br$) of 1.26 T and an intrinsic coercivity ($bHc$) of 960 kA/m. Figure 6b presents a comparison of the calculated axial magnetic field generated by the permanent magnet and the electromagnet. In the case of the permanent magnet, the presence of a magnetic null point results in a different axial magnetic field profile compared to that of the electromagnet. The magnetic flux density at the cathode tip is 0.175 T for the permanent magnet, while for the electromagnet, it is 0.016 T, 0.049 T, and 0.065 T at coil currents of 10 A, 30 A, and 40 A, respectively. In the permanent magnet configuration, FEMM simulations show that the axial magnetic field decays to near zero at an axial distance of approximately 7 cm from the cathode tip, indicating a significantly shortened effective magnetic field compared to the electromagnet configuration. Figure 6c illustrates the magnetic field distributions simulated using Finite Element Method Magnetics (FEMM) for both the electromagnetic and permanent magnet configurations. The results indicate that the axial magnetic field is dominant within the discharge channel in the electromagnet configuration, whereas in the permanent magnet configuration, the presence of a magnetic null point leads to an increased radial magnetic field near the magnet. Specifically, near the magnetic null point, located approximately 6 cm above the cathode–anode center, the permanent magnet configuration exhibits a substantial radial magnetic field, with the radial-to-axial field ratio reaching approximately 2. At the corresponding location, the electromagnet configuration shows a much weaker radial component, with the radial-to-axial field ratio remaining below 0.2.

*Thrust measurement system and vacuum facilities.* To evaluate the performance of the AF-MPD thruster, a plate spring-type thrust stand equipped with a load cell was used. The plasma source was mounted on the stand, which was supported by four plate springs[19]. The load cell was calibrated by hanging 10 g weights using a pulley system. The thrust was calculated from the average of the linear-fitted calibration data obtained before and after the experiments, with a calibration uncertainty below 3%. As a representative operating condition, at an input power of 10 kW and an argon flow rate of 1000 sccm, repeated thrust measurements showed a mean thrust of 310 mN with an uncertainty of ± 23 mN, corresponding to 7.4%. This total uncertainty was obtained by combining the calibration uncertainty and the uncertainty associated with plasma reproducibility using a root-sum-square method. When a thrust is generated in the direction opposite to the ion acceleration, the load cell converts this thrust into an electrical signal proportional to the applied thrust. The measurable thrust ranges from 0.1 N to 1 N. Calibration coefficients were calculated by averaging the results obtained from pre- and post-experiment calibrations.

The experiments took place in a cylindrical vacuum chamber made of stainless steel, with a diameter and length of 1.5 m, as shown in Fig. 7a. The thrust measurement system employed in the experiment is presented in Fig. 7b. The vacuum system consisted of four turbopumps and two cryopumps, with a pumping speed of 11,000 L/s for argon. During operation, the system maintained a pressure below 1.7 mTorr at an argon flow rate of 1000 sccm. During operation, pressure fluctuations were maintained within ±0.1 mTorr, and no significant influence on the I–V characteristics or thruster performance was observed.

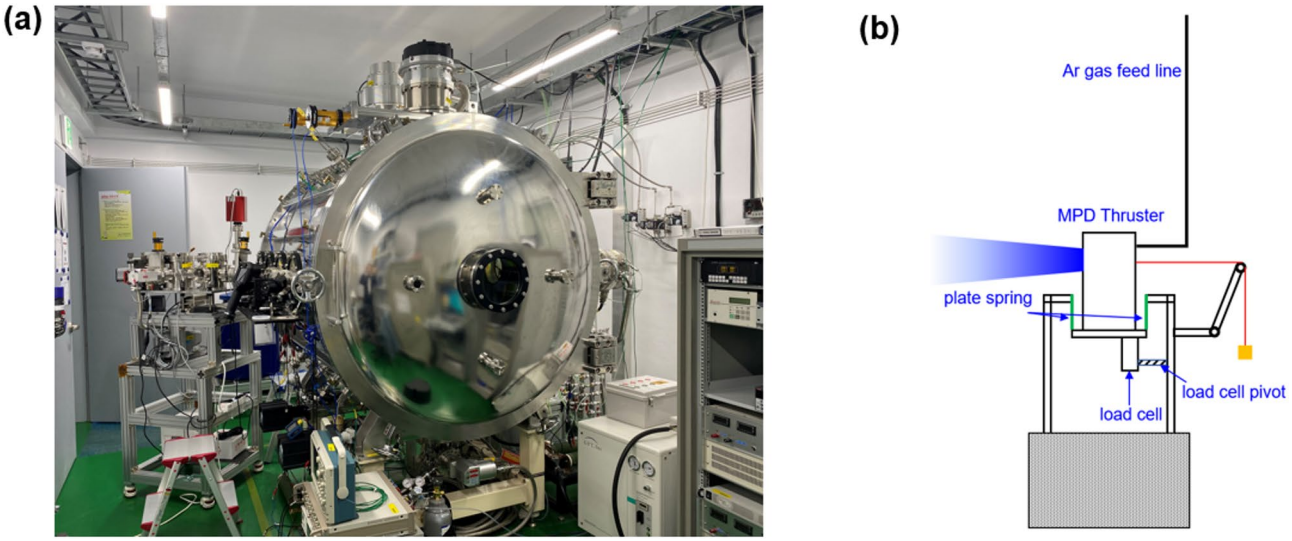


**Fig. 7**. (**a**) Photograph of the experimental setup inside the vacuum chamber and (**b**) schematic diagram of the AF-MPD thruster performance measurement system.

## Data availability

The datasets used and/or analysed during the current study available from the corresponding author on reasonable request.

Received: 19 May 2025; Accepted: 29 January 2026
Published online: 06 February 2026

## References

1. Goebel, D. M., Katz, I. & Mikellides, I. G. Fundamentals of electric propulsion. Wiley (2023).
2. Ahangar, M., Ebrahimi, R. & Shams, M. Numerical simulation of non-equilibrium plasma flow in a cylindrical MPD thruster using a high-order flux-difference splitting method. *Acta Astronaut.* **103**, 129–141 (2014).
3. Albertoni, R., Paganucci, F. & Andrenucci, M. A phenomenological performance model for applied-field MPD thrusters. *Acta Astronaut.* **107**, 177–186 (2015).
4. Krulle, G., Auweter-Kurtz, M. & Sasoh, A. Technology and application aspects of applied field magnetoplasmadynamic propulsion. *J. Propul. Power*. **14** (5), 754–763 (1998).
5. Sasoh, A. et al. Electrostatic-magnetic-hybrid thrust generation in central–cathode electrostatic thruster (CC–EST). *Acta Astronaut.* **152**, 137–145 (2018).
6. Tauchi, S., Oshio, Y., Kawasaki, A., Kubota, K. & Funaki, I. Analysis of thrust performance and cathode phenomena on a megawatt-class MPD thruster, AIAA SciTech 2019 Forum, p. 1241. (2019).
7. Nerheim, N. M. & Kelly, A. J. *A Critical Review of the Magnetoplasmadynamic (MPD) Thrustor for Space Applications* (Jet Propulsion Laboratory, California Institute of Technology, 1968).
8. Brophy, J. Advanced ion propulsion systems for affordable deep-space missions. *Acta Astronaut.* **52** (2–6), 309–316 (2003).
9. Mikellides, P. G. Modeling and analysis of a megawatt-class magnetoplasmadynamic thruster. *J. Propul. Power*. **20** (2), 204–210 (2004).
10. Patel, S., Bondugula, M. & Gorakula, S. MPD thruster technology and its limitations. *Int. J. Sci. Adv.* **2** (4), 578–585 (2021).
11. Cassady, R. J. et al. Recent advances in nuclear powered electric propulsion for space exploration. *Energy. Conv. Manag.* **49** (3), 412–435 (2008).
12. La Rosa Betancourt, M. A., Bögel, E., Collier-Wright, M. R., Wilcox, J. & Kaplan, P. Comparative overview of NEP programs and concepts for human exploration missions, **ASCEND 2021** 4075. (2021).
13. McGuire, M. L., Borowski, S. K., Mason, L. M. & Gilland, J. *High Power MPD Nuclear Electric Propulsion (NEP) for Artificial Gravity HOPE Missions To Callisto* (Space Technology and Applications International Forum, 2003).
14. Gibson, M. A., Oleson, S. R., Poston, D. I. & McClure, P. NASA's Kilopower reactor development and the path to higher power missions. In 2017 IEEE aerospace conference, IEEE, pp. 1–14. (2017).
15. Venneri, P. & Eades, M. Space nuclear power and propulsion at USNC-Tech. *Nucl. Technol.* **207** (6), 876–881 (2021).
16. Duchek, M. E. et al. Nuclear electric propulsion for Saturn and enceladus science missions. *J. Electr. Propuls.* **4** (1), 54 (2025).
17. Sasoh, A. & Arakawa, Y. Electromagnetic effects in an applied-field magnetoplasmadynamic thruster. *J. Propul. Power*. **8** (1), 98–102 (1992).
18. Arakawa, Y. & Sasoh, A. Steady-state permanent magnet magnetoplasmadynamic thruster. *J. Propul. Power*. **5** (3), 301–304 (1989).
19. Shin, H., Chai, K. B. & Kim, H. Performance and discharge characteristics of Applied–Field MPD thruster in accordance with ring magnet position. *Vacuum* **230**, 113674 (2024).
20. Krülle, G. Characteristics and local analysis of MPD thruster operation. In 6th Electric Propulsion and Plasmadynamics Conference, p. 672. (1967).
21. Boxberger, A. & Herdrich, G. Experimental test campaign of gas-fed steady state applied-field magnetoplasmadynamic Thruster SX3, IEPC Paper 251 2013. (2013).
22. Lev, D. R. & Choueiri, E. Y. Scaling of efficiency with applied magnetic field in magnetoplasmadynamic thrusters. *J. Propul. Power*. **28** (3), 609–616 (2012).
23. Polzin, K. et al. Performance of a permanent-magnet cylindrical Hall-effect thruster. In 45th AIAA/ASME/SAE/ASEE Joint Propulsion Conference & Exhibit, p. 4812. (2009).

24. Ferreira, J. L. et al. Permanent magnet hall thruster development for future Brazilian space missions. *Comput. Appl. Math.* **35**, 711–726 (2016).
25. Polzin, K., Raitses, Y., Gayoso, J. & Fisch, N. Comparisons in performance of electromagnet and permanent-magnet cylindrical hall-effect thrusters. In 46th AIAA/ASME/SAE/ASEE Joint Propulsion Conference & Exhibit, p. 6695. (2010).
26. Auweter-Kurtz, M., Kriille, G. & Kurtz, H. The investigation of applied-field MPD thrusters on the international space station. In Proc. 25th Int. Electr. Propuls. Conf.(IEPC), pp. 721–727. (1997).
27. Collier-Wrighta, M., Bögela, E., Betancourta, M. L. R., Behnkeb, A. & Herdrichb, G. Progress in research and development of superconductor-based applied-field magnetoplasmadynamic technology marcus collier-wrighta, Elias Bögela, Manuel La Rosa Betancourta (2021).
28. Maeshima, D., Mori, R., Inoue, S., Tsuchiya, Y. & Kinefuchi, K. MPD thruster with a strong applied field up to 0.5 T using cryogenic fluid-cooled magnetic coil. *J. Electr. Propuls.* **4** (1), 1–12 (2025).
29. Wanke, D. et al. Facility Advancement and Mapping for the Advanced 5 kW AF-MPD Thruster SUPREME. In The 38th International Electric Propulsion Conference, 2024.
30. Sun, Y. et al. Experimental investigation of the electromagnetic acceleration mechanisms in an applied-field magnetoplasmadynamic thruster. *Plasma Sources Sci. Technol.* **33** (11), 115016 (2024).
31. Du, Y. et al. Theoretical research on magnetic confinement mechanism of applied-field magnetoplasmadynamic thruster. *Aerospace* **10** (2), 124 (2023).
32. Reece, J. Roth, Industrial plasma engineering, IOP (1995).
33. Kodys, A. & Choueiri, E. A critical review of the state-of-the-art in the performance of applied-field magnetoplasmadynamic thrusters. In 41st AIAA/ASME/SAE/ASEE Joint Propulsion Conference & Exhibit, p. 4247. (2005).
34. Kim, H., Doh, G. & Choe, W. Generation of multiply charged ions in accordance with geometry and magnetic field in hall thruster plasmas. *Curr. Appl. Phys.* **51**, 8–12 (2023).
35. Kim, H., Lim, Y., Choe, W., Park, S. & Seon, J. Effect of magnetic field configuration on the multiply charged ion and plume characteristics in hall thruster plasmas. *Appl. Phys. Lett.* **106**(15) (2015).
36. Tikhonov, V., Semenikhin, S., Brophy, J. & Polk, J. Performance of 130 kW MPD thruster with an external magnetic field and Li as a propellant. In Proceedings of the 25 th International Electric Propulsion Conference, pp. 728–733. (1997).
37. Mikellides, P. & Turchi, P. A theoretical model for the thrust and voltage of applied-field MPD thrusters. In 34th AIAA/ASME/SAE/ASEE Joint Propulsion Conference and Exhibit, p. 3474. (1998).
38. Tahara, H., Kagaya, Y. & Yoshikawai, T. Effects of applied magnetic fields on performance of a quasisteady magnetoplasmadynamic Arc. *J. Propul. Power*. **11** (2), 337–342 (1995).
39. Chai, K. B. & Kwon, D. H. Heat and particle load test facility using an applied-field MPD thruster for studying fusion divertor technology. *Plasma Phys. Controlled Fusion*. **62** (3), 035007 (2020).
40. Chai, K. B., Kwon, D. H. & Lee, M. Development of plasma beam irradiation facility using applied-field MPD thruster to study plasma-surface interactions. *Plasma Phys. Controlled Fusion*. **63** (12), 125020 (2021).


## Acknowledgements

This work was partially supported by National R&D program through the National Research Foundation of Korea (NRF) funded by Ministry of Science and ICT (RS-2022-00155950) and by KAERI Institutional Program (524560-25). This work was also partially supported by "A Research on Critical Technology for Scalable Space Tug with Autonomy and Reconfigurability" of Korea Aerospace Research Institute (Grand No. FR25F00).

## Author contributions

The original draft was written by H.S., who also conducted the methodology design, investigation, visualization, and data curation. Data curation support was provided by J.K., J.H., and K.C. Review and editing of the manuscript were performed by J.K., J.H., K.C., and H.K. Validation was carried out by K.C. and H.K. Methodology development was led by H.S. and H.K. Supervision and funding acquisition were provided by K.C. and H.K. All authors reviewed the first and final manuscript.

## Funding

This work was partially supported by National R&D program through the National Research Foundation of Korea (NRF) funded by Ministry of Science and ICT (RS-2022-00155950) and by KAERI Institutional Program (524560-25). This work was also partially supported by "A Research on Critical Technology for Scalable Space Tug with Autonomy and Reconfigurability" of Korea Aerospace Research Institute (Grand No. FR25F00).

## Declarations

## Competing interests

The authors declare no competing interests.

## Additional information

**Correspondence** and requests for materials should be addressed to K.-B.C. or H.K.